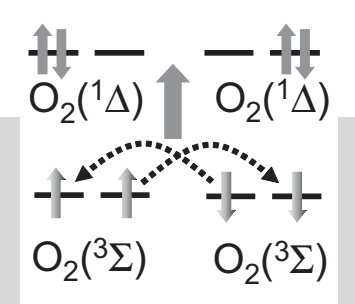
nlinelibary.wiley.com/doi/0.10.002/adma.200500328 by Egyptia Marional Sti. Network (Enstinet), Wiley Online Library on [12.03/2023]. See the Terms and Conditions (https://onlinelibrary.wiley.com/terms-and-conditions) on Wiley Online Library for rules of use; OA articles are governed by the applicable Creat

Silicon Nanocrystals: Photosensitizers for Oxygen Molecules**

By *Dmitri Kovalev** and *Minoru Fujii*

Molecular oxygen plays an important role in many of the chemical reactions involved in the synthesis of biological life. In this review, we explore the interaction between O_2 and silicon nanocrystals, which can be employed in the photosynthesis of singlet oxygen. We demonstrate that nanoscale Si has entirely new properties owing to morphological



and quantum size effects, i.e., large accessible surface areas and excitons of variable energies and with well-defined spin structures. These features result in new emerging functionality for nanoscale silicon: it is a very efficient spin-flip activator of O_2 , and therefore, a chemically and biologically active material. This whole effect is based on energy transfer from long-lived electronic excitations confined in Si nanocrystals to surrounding O₂ via the exchange of single electrons of opposite spin, thus enabling the spin-flip activation of O_2 . Further, we discuss the implications of these findings for physics, chemistry, biology, and medicine.

1. Introduction

Molecular oxygen and silicon are the two most common substances on earth. A variety of chemical reactions involving O₂ are crucial for chemical and biological systems, while Si plays an important role in modern technology. The direct excitation of the chemically, and therefore biologically, inert ground triplet state of O₂ to the highly reactive excited singlet states by photons is forbidden by the spin selection rule. The spin selection rule governs the likelihood that a physical system will change from one state to another or determines if it will be unable to make such a transition. Recently, it has been realized that the spin states of energetically or chemically interacting substances can substantially control the interaction process between them. One of the most important examples is the interaction of organic molecules with O₂. The interest that O2 has attracted in various scientific fields, e.g., molecular physics and photochemistry, stems from its particular electronic configuration. It is well known that the ground state of O_2 is the triplet state $(^3\Sigma)$. [1,2] Chemical reactions between singlet organic molecules and triplet O2 to form new singlet organic molecules are forbidden by Wigner's spin selection rule. Thus, the triplet multiplicity of O_2 is the reason why most reactions between oxygen and organic substances do not occur at room temperature, i.e., they are kinetically inhibited. In general, consideration of spin-conservation restrictions answers a fundamental question: why is organic life so stable in the ubiquitous presence of chemically active oxygen?

The two lowest excited states of O_2 are singlets, $^1\Delta$ and $^{1}\Sigma$. [1,2] The corresponding electron spin configurations of these states, and gaps between the energy levels, are indicated in Figure 1a. Kautsky and DeBruijn first experimentally demonstrated the existence of singlet-oxygen molecules (¹O₂).^[3] Because of its singlet multiplicity, no spin restriction exists for reactions of ¹O₂ with singlet organic molecules. This, combined with their excitation energies of 0.98 and 1.63 eV,

Department of Electrical and Electronics Engineering Faculty of Engineering, Kobe University Rokkodai, Nada, Kobe, 657-8501 (Japan)

[**] We thank the many colleagues and co-workers who have contributed ideas, theoretical and experimental work, and are not formally authors of this review. In particular, Egon Gross, Joachim Diener, Nicolai Künzner, and Viktor Timoshenko deserve mention here. A part of this work was supported by the Industrial Technology Research Grant Program from the New Energy and Industrial Technology Development Organization (NEDO), Japan and by Commission of the European Communities, 6th Framework Program (STRP 013875).

^[*] Dr. D. Kovalev Physics Department, Technical University of Munich D-85748 Garching (Germany) E-mail: dkovalev@ph.tum.de Dr. M. Fujii

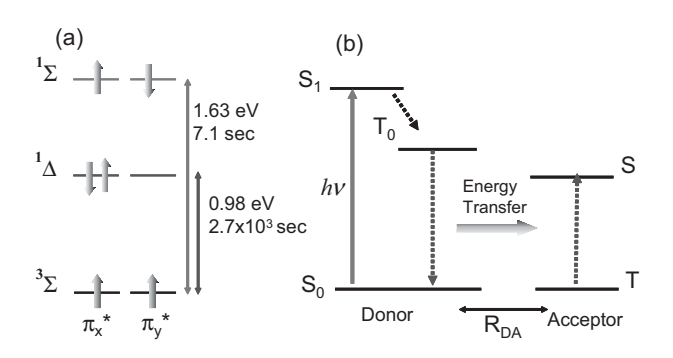


Figure 1. a) Electronic spin configurations and spectroscopic labeling of molecular oxygen states. The excitation energies and intrinsic lifetimes of the $^1\Sigma$ and $^1\bar{\Delta}$ states of O_2 are also shown. b) Schematic illustration of the energy-transfer process between the light-absorbing donor and the acceptor. S denotes a singlet state and T denotes a triplet state. h: Planck's constant; v: frequency of photons; RDA: space separation between the donor and O2.

makes ¹O₂ extremely chemically reactive. The singlet states mediate fundamental processes in chemistry and biology. [4-6] They react with many organic compounds including aromatics, steroids, vitamins, amino acids, proteins, etc. They are applied in bleaching and disinfection reactions, and are also involved in the modification of biological structures.^[7,8] Some examples of the latter include lipid peroxidation and photohemolysis. An important example of the medical applications of ¹O₂ is the photodynamic therapy of cancer. ^[6]

¹O₂ can be produced via gaseous discharge or chemical reactions. [2,7] However, large varieties of practical applications, especially in medicine, require its generation in organic solvents or human tissue in a controlled manner. Therefore, the most common ¹O₂-generation procedure involves photosensitizers. [1,2] Photosensitization is an important process employed for the excitation of molecules exhibiting optically forbidden electronic transitions. The transition from the $^{3}\Sigma$ ground state to one of the excited ¹O₂ states, and vice versa, requires a change of the electron spin state (spin-flip process). However, direct conversion of spin states via the absorption/emission of photons is spin-forbidden in the first approximation. [1,2] This causes extremely long radiative lifetimes for the $^{1}\Delta$ and $^{1}\Sigma$ states, being 2.7×10^3 and 7.1 s, respectively. [1,2]

To overcome this problem with direct photoexcitation, several auxiliary agents, called "photosensitizers", e.g., strongly absorbing organic dye molecules, are commonly used. [1,2] As a result of light absorption, the dye molecules are excited into an optically active singlet state, and after relaxation they are accumulated in the long-lived triplet state (Fig. 1b). Further energy transfer from the excited dye molecules (donor) to O₂ (acceptor) proceeds via dipole–dipole (Förster) processes^[9] or direct electron-exchange interactions (Dexter processes).^[10] Interaction of the excited triplet state of the dye molecule with the triplet ground state of O₂ results in relaxation of the dye molecule to the ground state, while O2 is activated via a spin flip. In both scenarios, a few key requirements have to be fulfilled to ensure high efficiency of energy transfer. [1,2] First, the excited triplet state of the photoexcited donor must have



Dr. Dmitri Kovalev received his Ph.D. at A. F. Ioffe Physico-Technical Institute (PTI), St. Petersburg, Russia in 1989. From 1989 to 1994 he worked as a research associate at PTI. In 1994 he joined the Physics Department of the Technical University of Munich (TUM) as a Fellow of the Alexander von Humboldt Foundation. Since 1996 he has been working at TUM firstly as a scientist, and, after finishing his habilitation in 2001, as a senior scientist.



© 2005 WILEY-VCH Verlag GmbH & Co. KGaA, Weinheim

Dr. Minoru Fujii received his Ph.D. at Kobe University, Japan. He was awarded the "Young Authors Best Paper Award" at the 20th International Conference on the Physics of Semiconductors, Thessaloniki (Greece) in 1990. After finishing his Ph.D., he joined Matsushita Electric Industrial Co., Ltd. (Panasonic). In 1995, he started work at Kobe University as a research associate. From 2001 to 2002, he was in the group of Dr. D. Kovalev at the TUM under a fellowship of the Alexander von Humboldt Foundation. He is now an Associate Professor at Kobe University.

15214095, 2005, 21, Downloaded from https://onlinelibrary.iley.com/doi/1.01002adma_200500328 by Egyptin Marianal St. Network (Estinated, Wiley Online Library on 1120302033). See the Terms and Conditions (https://onlinelibrary.wiely.com/terms-and-conditions) on Wiley Online Library for rules of use; OA articles are governed by the applicable Creative Commons

2533 ₺

ADVANCED

a longer lifetime compared with the energy-transfer time. Second, the allowed energies of the donor should match those of the singlet states of O₂. Finally, space separation between the donor and $O_2(R_{DA})$ should be small. Other desirable features include readily available light sources for the selective excitation of the sensitizer.^[1,2]

Over the last few decades, a large number of different substances that are able to generate singlet-oxygen molecules and hundreds of photochemical reactions involving oxygen molecules have been studied. Efficiencies for the sensitized generation of ¹O₂ have been determined for hundreds of photosensitizers, [1-3] because of the importance of ¹O₂ as a chemical reagent. Specifically, for the photodynamic therapy of cancer, typical photosensitizers used are members of a family of dye molecules known as porphyrins. [6] These compounds have properties that are crucial for photodynamic therapy; they are soluble in water, stable under illumination, non-toxic, and able to efficiently absorb visible light. Because of the small diffusion length of singlet oxygen in water, their action is localized to the area where the photosensitizer is located and where it is excited by light. A strong limitation of photodynamic therapy is the poor penetration of light into tissue. Owing to strong light absorption and scattering in human tissue, only light with a wavelength longer than 650 nm has the ability to penetrate relatively deeply into the human body. The current generation of photosensitizers efficiently absorb light between 630 and 700 nm, which penetrates only a few millimeters into tissue. To overcome this limitation, researchers are synthesizing new compounds, which will be able to absorb light in the 700-800 nm wavelength range, and penetrate to depths of a few centimeters.

One of the strategic objectives of nanotechnology is the development of new materials of nanometer size that have entirely new physical properties, and, therefore, new functionality. Only recently has the generation of singlet oxygen by semiconductor nanocrystals (quantum dots) and nanoparticles, including fullerenes and their derivatives, received significant attention. [11–14] Unfortunately, since C_{60} and C_{70} fullerenes do not absorb photons effectively in the visible and near-infrared region of the electromagnetic spectrum, their potential use as in-vivo sensitizers can be considered only if an addend acting as a light-harvesting antenna is appended to their skeleton.[15]

The optical and electronic properties of traditional semiconductors are difficult to adjust, because their bandgap and emission energies are not easily changeable. Over the last decade, tailoring of material characteristics by size control has been demonstrated for many types of semiconductors. Semiconductor nanocrystals contain from a few hundreds to a few tens of thousands of atoms that are arranged in an orderly way, following the crystalline structure of the bulk material. Their optical and electronic properties can be engineered simply by changing their size and composition. [16–18] When electrons and holes are squeezed into a dimension that approaches a critical size, called the exciton Bohr radius in the bulk material, quantum-confinement effects become apparant. In this regime, electron and hole energy levels have to be treated as discrete, and reduction of nanocrystal size leads to a larger energy separation between the lowest electron and hole states. [18] This effect can be seen experimentally as a widening of the nanocrystal bandgap. For instance, size reduction of CdSe nanocrystals from 4 to 2.1 nm is accompanied by a 0.5 eV blue-shift in their bandgaps and emission energies.^[19] Thus, by using different semiconductor nanocrystals, the entire visible and near-infrared spectral range of the electromagnetic spectrum, as opposed to the visible range of conventional ¹O₂ photosensitizers, can be covered.

Under normal conditions, most semiconductor nanocrystals have direct bandgaps, and therefore the rate of radiative recombination of excitons is extremely large if the optical transition is dipole-allowed. However, theory predicts that the lowest exciton state of direct-bandgap CdSe nanocrystals is a triplet state, [20] frequently referred to as a "dark state". This result is potentially important because the triplet structure of excitons is necessary for energy transfer from excitons to O2 to occur, in a manner similar to that of dye molecules. Unfortunately, in direct-bandgap semiconductors, owing to a small singlet-triplet splitting energy, the exciton lifetime at room temperature is controlled by thermally excited, optically allowed singlet "bright" states and is in the submicrosecond time domain.^[21] It is necessary to note that in photosynthesis the time for energy transfer to the acceptor always competes with the lifetime of the electronic excitations of the donor. Therefore, the fast relaxation of excitons would drastically reduce the photosensitizing ability of direct-bandgap nanocrystal assemblies, [22] and their application potential in the generation of ¹O₂ is questionable.

Since 1990, [23] several approaches have been developed towards improving the efficiency of light emission from nanosilicon-based structures. Recently, it has been recognized that despite tunable photoluminescence (PL) and a high quantum yield, a long exciton lifetime is the inherent limitation for light-emitting applications of Si nanocrystal assemblies. [23,24] However, only recently has it been understood that this is certainly a great advantage for photosensitizing applications. Above, we have formulated the key requirements for photosensitizing substances. According to these criteria, Si nanocrystals seem to be almost ideal candidates for use as donors for efficient energy transfer to O₂. Indeed, by adjusting the size of Si nanocrystals, the energies of the confined excitons can be tuned over a wide range. The ground state of the excitons is a triplet state and the lifetime of indirect-bandgap excited singlet exciton states, contrary to those of direct-bandgap nanocrystals, is extremely long. Finally, Si nanocrystal assemblies have a huge internal area (as much as 500 m² cm⁻³) accessible to O_2 . We have found recently that this combination of new physical properties of Si at the nanoscale is exceptionally favorable for the transfer of energy from photoexcited Si nanocrystals to O2, and the efficiency of this process is approximately 100 % at low temperatures. [25]

The overall goal of this review is to survey experimental work that has been performed towards developing a detailed

ADVANCED MATERIALS

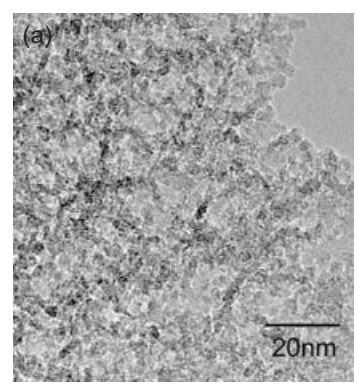
understanding of energy transfer from photoexcited Si nanocrystals to O_2 . The first part of this paper will cover issues related to the well-studied morphological and optical properties of Si nanocrystal assemblies, which, owing to quantum-confinement effects, are completely different from those of bulk Si. In the second part, we will describe the interactions between excitons confined in Si nanocrystals and O_2 in the gas phase or dissolved in liquids. We demonstrate that the unique optical properties of Si nanocrystals allow investigation of the mechanism of energy transfer in much more detail than for ordinary photosensitizers. Finally, possible implications of the observed phenomena for physics, chemistry, and biology and the arising problems will be discussed.

2. Morphology of Si Nanocrystal Assemblies

As a result of its indirect-bandgap electronic structure, bulk Si is a spectacularly inefficient light emitter. In recent years, several technological approaches have been developed towards improving the efficiency of light emission from different systems containing Si nanocrystals. All of them rely on the lifting of bulk Si lattice periodicity inducing an uncertainty in the crystal momentum space, thereby altering the indirect nature of this material. Si nanocrystal assemblies can be prepared in different ways. Some examples include aerosol procedures^[26] and the thermal precipitation of Si atoms implanted in SiO₂^[27-29] or Si–SiO₂ superlattices.^[30] Recently, laser-pyrolysis techniques have been introduced to achieve a relatively narrow size distribution of Si nanocrystals.^[31] The most widely discussed system in the literature is porous silicon (PSi). [23,32-34] The anodization of bulk Si wafers is performed in HF-based solutions. Depending on the type of wafer doping (p- or n-type) and the doping level, the sizes of the pores and remaining Si fragments can be varied from micro- to nanometers. [23,35] This has attracted much interest owing to the simplicity of the preparation procedure that requires neither lithographic nor epitaxial techniques, which used to be the conventional approaches for obtaining nanometer-sized semiconductor structures. Here, we will concentrate only on the properties of nanoporous Si layers that exhibit a high emission efficiency (up to 10%) under optical excitation, due to quantum confinement effects.

Figure 2 shows typical transmission electron microscopy (TEM) images of nanoporous Si. Electrochemical or stain etching of p-doped bulk Si wafers^[36,37] results in a sponge-like structure that consists of Si nanocrystals of different sizes.^[38] They are typically a few nanometers wide, as can be seen in Figure 2a, and retain the diamond lattice structure of bulk Si (Fig. 2b, the lattice fringes correspond to (111) planes of Si nanocrystals).^[37] As a result, PSi is characterized by a very large internal surface area.^[39] Hydrogen atoms passivate the internal surface of as-prepared materials, which reduces the number of non-radiative surface defects such as dangling Si bonds.^[23] Native oxidation on a time scale of months, or intentional oxidation in the temperature range 200–300 °C,

© 2005 WILEY-VCH Verlag GmbH & Co. KGaA, Weinheim



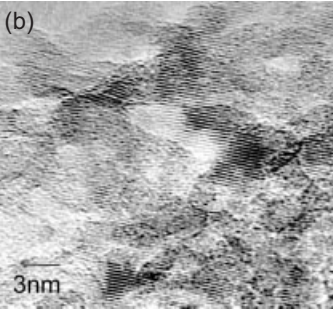


Figure 2. TEM images of PSi at different magnifications. The lattice fringes in Fig. 2b correspond to (111) planes in the Si nanocrystals.

builds up one monolayer of oxygen atoms back-bonded to the surface layer, which prevents further surface oxidation. At temperatures above 300 °C, hydrogen effuses from the surface of the nanocrystals, and they become oxygen-terminated. [23] Another essential morphological property of PSi layers is that all the pores are interconnected, which enables foreign substances to be incorporated in the pores.

3. Emission Properties of Si Nanocrystals

Historically, worldwide interest in PSi appeared primarily after the discovery by Canham that highly porous Si structures emit light very efficiently in the visible and near-infrared range of the electromagnetic spectrum at room temperature.[32] Independently, Lehmann and Gösele reported that the absorption properties of PSi in the visible spectral range are strongly modified.^[33] The authors of these studies proposed that the observed behavior arises from quantum-confinement effects. This discovery was followed by hundreds, probably even thousands, of experimental and theoretical publications (see previous reviews and references therein)[23,24,34] devoted to this issue. According to the inventors, this enormous interest appeared "because Si is the most technologically important material known to mankind, dominating the microelectronics revolution that influences our everyday lives. Light-emitting Si devices could eventually result in a new generation of Si chips and extend the functionality of Si technology from microelectronics into optoelectronics". [23] It

15214095, 2005, 21, Dwnloaded from https://onlinelibaray.wiley.com/doi/1.01002/ahma.200500328 by Egyptin Marianal St. Network (Estinated, Wiley Online Library on [1232023]. See the Terms and Conditions (https://onlinelibaray.wiley.com/emand-conditions) on Wiley Online Library for rules of use; OA articles are governed by the applicable Creative Commons

has since been demonstrated that all systems containing Si nanocrystals exhibit strong near-infrared and visible PL with characteristics very similar to those of PSi. Recently, however, an inherent complication arising from the very specific nature of the optical transitions and morphology of the material has been recognized.

Clear evidence that the emitting states of Si nanocrystals are driven to higher energies by quantum-confinement effects can be derived from measurements of PL resulting from excitation by high-energy photons, when all crystallites in the distribution are excited. Figure 3 demonstrates PL spectra from different types of Si nanocrystal assemblies. The PL, depending on the mean size of the Si nanocrystals, can be continuously tuned with small increments over a very wide spectral

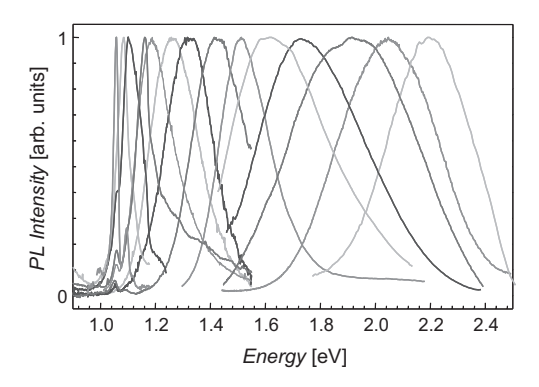


Figure 3. Tunability of the PSi PL band. To achieve size variation of Si nanocrystals, different levels of bulk Si substrate doping and various etching parameters (current density and etching solution concentration) have been used. Excitation energy, $E_{ex} = 2.54$ eV.

range, from the bulk-Si bandgap to the green region of the electromagnetic spectrum for the smallest nanocrystals. Thus, the confinement energy can be more than 1 eV, i.e., as large as the fundamental silicon bandgap itself. This observation is crucial since it implies that the energy of the excitons can be adjusted to any desirable value from 1 to 2.5 eV, simply by selecting the appropriate size of Si nanocrystal. These spectra (with full widths at half maximum of up to 500 meV) differ greatly from those known for other quantum-dot systems. No distinct emission features that could allow the determination of the nature of the luminescent centers are observed. This discrepancy has stimulated a wide variety of models to explain the physical mechanism of emission from Si nanocrystals. Cullis et al. have published a detailed discussion of the various proposed models.^[23] Calcott et al. found the key spectroscopic argument supporting the original quantum confinement model in 1993. [40] It was natural to assume that the large line width of the PL band is a direct consequence of the residual nanocrystal size and shape distributions. Calcott et al. employed a standard PL line-narrowing technique widely used in optical spectroscopy to lift the inhomogeneous PL line broadening.^[40] The essence of this approach is the selectivity of the optical excitation. The low-energy part of the ordinary PL band is governed by emission coming from larger nanocrystals. When the energy of the exciting laser light is chosen to fall inside the low-energy part of the PL band, only a very small subset of nanocrystals, those with bandgaps below the laser energy, is probed. Under these conditions, distinct PL onsets or PL peaks can be observed. [40-45] It has been proposed that these PL signatures provide evidence that the luminescing material has the electronic and vibrational band structure of crystalline Si. [40] Figure 4a demonstrates the result of this type of experiment performed with PSi. For comparison, a PL spectrum of bulk crystalline Si is shown in Figure 4b. In bulk Si, owing to its indirect-bandgap nature, optical transitions are possible only if momentum-conserving phonons are emitted or ab-

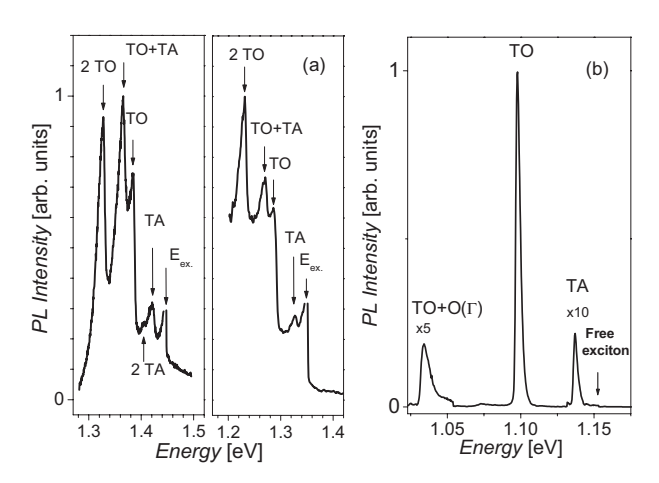


Figure 4. a) Resonant PL spectra of as-prepared (left) and heavily oxidized (right) PSi. The arrows show the energy position of silicon transverse acoustic (TA) and transverse optical (TO) momentum-conserving phonons with respect to the exciton ground state. T=1.3 K. The laser line position is indicated by E_{ex} . (Reprinted with permission from [44]. Copyright 1998 The American Physical Society). b) PL spectrum of undoped bulk silicon at T=20 K, $E_{\rm ex}=2.54$ eV. Momentum-conserving PL replicas of the free-exciton transition are indicated.

sorbed in the recombination process. This process has an extremely low probability, and therefore bulk Si is a very poor light emitter. At low temperatures, phonons can only be emitted and the two PL lines seen in Figure 4b are momentum-conserving replicas of the momentum-forbidden free-exciton transitions in bulk Si. Their energies with respect to the free-exciton emission energy position correspond to the energies of the momentum-conserving transverse optical (TO) phonon (56 meV) and the transverse acoustic (TA) phonon (18 meV) of bulk Si. Emission spectra from resonantly excited Si nanocrystals are very similar but the PL peaks are duplicated (see Fig. 4a). The observation of a peak structure in the resonant spectrum of an inhomogeneously broadened system of nanocrystals deserves further explanation. As mentioned before, spatial confinement partially breaks down the momentum-conservation rule and allows electronic transitions that involve no phonons. Therefore, in both absorption and emission, no-phonon and phonon-assisted transitions are possible. In Figure 5 we sketch for clarity three different groups of Si nanocrystals, which contribute to certain PL

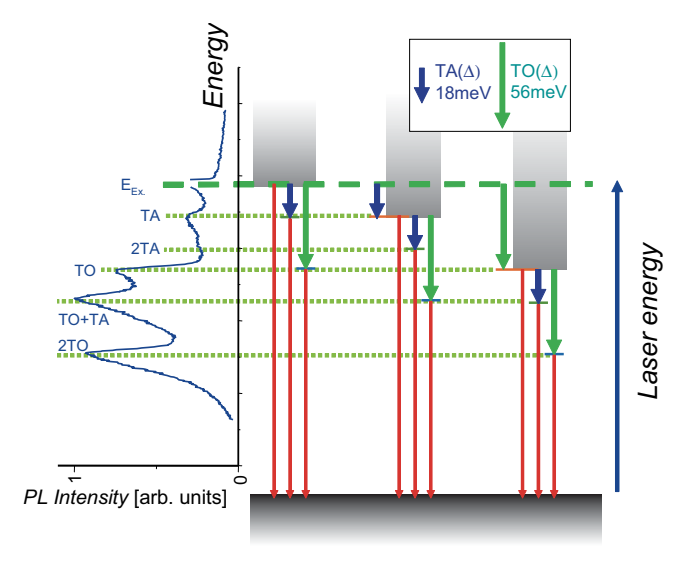


Figure 5. Sketch representing three groups of Si nanocrystals that have different bandgaps involved in absorption-emission cycles under resonant optical excitation. Arrows indicate momentum-conserving phonons participating in this cycle. Green arrows: emission of TO momentumconserving phonons. Blue arrows: emission of TA momentum-conserving phonons. The energy of the laser is indicated by a horizontal green dashed line. Red arrows demonstrate different recombination channels in Si nanocrystals. Left: each peak in the PL spectrum corresponds to additional no-phonon and phonon-assisted processes in the absorptionemission cycle, which are allowed at this particular energy.

peaks under a certain excitation energy. At each specific energy, two groups of crystallites contribute to the emission, one of which has exactly this energy (recombination via no-phonon process) and the other which has larger bandgaps (TOand TA-phonon-assisted processes). The same is true for the absorption process. Thus, owing to the emission of phonons, the spectral features are replicated in energy. Each peak in the PL spectrum corresponds to additional no-phonon and phonon-assisted processes which are allowed at this particular energy in the absorption-emission cycle. Since only two strong PL peaks are observed (for each phonon), the possible transitions in the absorption-emission cycle involve zero, one, or two momentum-conserving phonons.

This finding was certainly the breakthrough in the controversial field of light emission from Si nanocrystals but the conclusions that can be drawn are extremely pessimistic. The overall concept of efficient light emission from nanosilicon relies entirely on the possibility of lifting crystalline momentum-conservation restrictions inherent in bulk Si. [46] When the size of the crystallite is so small that it contains only a few unit cells, any selection rule that derives from the translational symmetry of the bulk material crystalline lattice should be strongly broken. However, even nanometer-sized silicon crystallites do not become direct-bandgap semiconductors. Despite high PL yield, they still behave as indirect-bandgap semiconductors.

© 2005 WILEY-VCH Verlag GmbH & Co. KGaA, Weinheim

In bulk Si, the radiative lifetime of electron-hole excitations is extremely long and has never been measured experimentally. Their decay is almost completely controlled by a variety of fast non-radiative processes, which results in an extremely low optical-emission quantum yield. In contrast, the first measurements of the temporal evolution of the PL emitted by PSi have already revealed its extremely long decay time. The decay time of the PL was found to be in the microsecond range, compared to the nanosecond radiative lifetimes observed in low-dimensional direct-bandgap semiconductors. [46,47] In bulk semiconductors, each exciton can recombine non-radiatively owing to the presence of non-radiative defects and efficient exciton transport. The hydrogen or oxygen passivation of Si-nanocrystal surfaces reduces the number of surface recombination centers per unit area. Additionally, the transport of excitons in a nanocrystal network is strongly suppressed as a result of the presence of potential barriers. Thus, excitons mainly recombine within the nanocrystals in which they are created, i.e., recombination has a geminate character. [48,49] Therefore, the main reason for the high external quantum efficiency of the emission from PSi compared to that from bulk Si is not a reduction of the radiative lifetime of the excitons, but results specifically from the non-radiative recombination channels being "disabled". [23,24]

15214095, 2005, 21, Downloaded from https://onlinelibrary.wiley.com/doi/10.1002/adma.200500328 by Egyptin Marianal Sti. Network (Ensinet). Wiley Online Library on [12.032023]. See the Terms and Conditions (https://onlinelibrary.

conditions) on Wiley Online Library for rules of use; OA articles are governed by the applicable Creative Commons

Figure 6 demonstrates the spectral dependence of the PL decay time measured for PSi at 200 K, where the PL quantum yield has its maximum value. Therefore, the measured decay

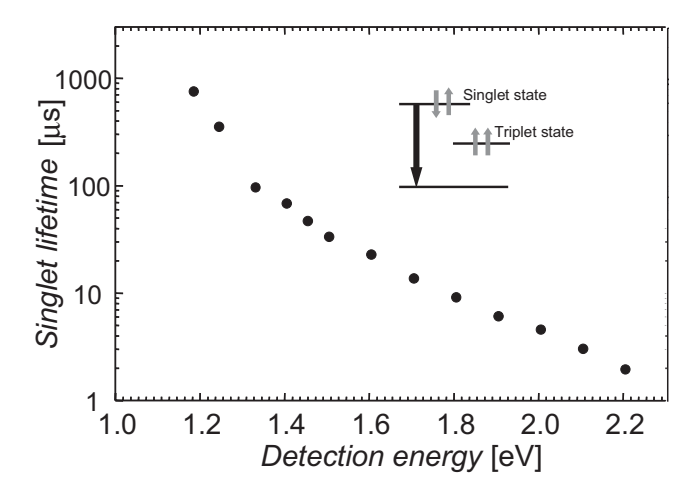


Figure 6. Spectral dispersion of the singlet-exciton lifetime. Inset: sketch of the splitting of exciton states due to electron-hole exchange interactions.

time, to a large extent, can be considered as a radiative one. The PL decay time varies from almost a millisecond near the bulk-Si bandgap to a microsecond for the green spectral range. The PL decay times measured for other systems containing Si nanocrystals have very similar values. A very strong spectral dispersion of the exciton recombination time is a di-



rect consequence of quantum-confinement effects. In smaller nanocrystals, quantum confinement increases the emission energy and also increases the oscillator strength of radiative transitions owing to a better overlap of electron and hole wavefunctions and breakdown of the translational symmetry, thus decreasing the radiative lifetime.

Study of the temporal PL behavior is important for determining the type of possible applications for which a particular luminescent material may be appropriate. A very long exciton lifetime is certainly a large disadvantage for light-emitting applications since the response of any device based on Si nanocrystals would be extremely long. On the other hand, long exciton lifetimes in the range 10^{-3} to 10^{-6} s implies very efficient storage of the energy of the electronic excitations, and therefore a possibility for efficient energy or charge transfer to other substances.

4. Spin Structure of Excitons Confined in Si **Nanocrystals**

The exchange interaction between electrons and holes that have a certain mutual spin orientation can be considered to be a very weak perturbation, and in bulk semiconductors only weakly modifies the electronic structure of the exciton. For instance, for the exciton in bulk Si, the exchange splitting energy is about 150 µeV and does not play a role in the optical transitions.^[50] Its value is strongly dependent on the spatial overlap of the electron and hole wavefunctions. When the size of the crystallite approaches the bulk exciton Bohr radius, a drastic enhancement of the effect is expected. Recently, it has been demonstrated that the electron-hole exchange interaction plays a crucial role in the description of the basic optical properties of nanocrystal assemblies and quantum dots.^[51–57] In most of these systems, the ground state of the exciton is "dark" as a result of exchange splitting. Lifetimes of the "dark" excitons are very long since the spin momentum of the exciton is equal to one, or in other words, it has a triplet nature. The first experimental evidence for the importance of this type of interaction in Si nanocrystals was provided by Calcott et al.[40] and was later confirmed by a number of different groups.^[58–60] The upper and lower exciton states are assumed to be an optically active spin singlet (S=0) and an optically passive spin triplet (S=1), respectively. Although spin-orbit interaction in Si is weak, it has been shown to play an important role in Si nanocrystals.^[59] Owing to this type of interaction, there is an admixture of singlet character in the triplet transitions and they become weakly allowed. [40,59] Despite the fact that this treatment of the structure of the exciton ground level in Si nanocrystals is simplified, it explains all the experimental observations very well.^[60]

In Figure 7, the resonant PL spectrum measured very near the excitation energy is shown. The spectral gap Δ_{exch} , of the order of a few millielectronvolts, between the excitation line and the onset of emission is clearly seen. This gap can be detected in all resonant PL spectra and its nature has been explained by Calcott et al. [40] Absorption takes place via the allowed singlet

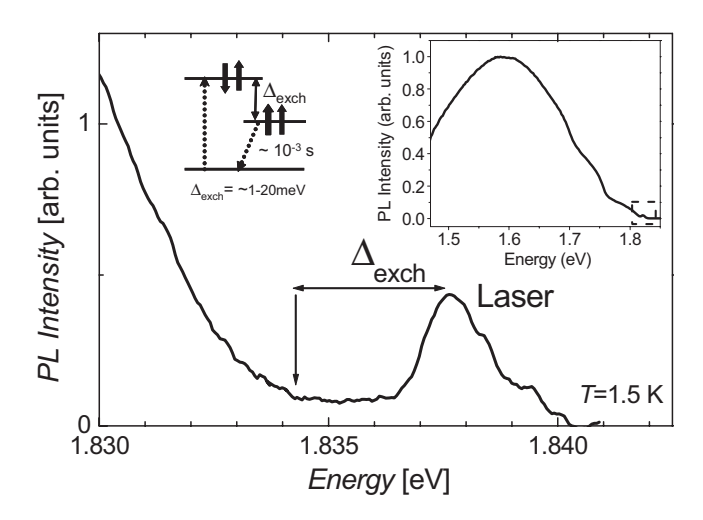


Figure 7. Resonant PL spectrum measured very near the excitation energy. The value of the spectral gap ($\Delta_{\rm exch}$) is indicated by a horizontal arrow. Left inset: sketch of exciton splitting owing to electron-hole exchange interactions. The spectral gap is indicated as Δ_{exch} . Right inset: resonant PL spectrum; the square is the area that has been magnified.

exciton state so long as the oscillator strength of this transition is high. At low temperatures, after a fast spin-flip process, the exciton relaxes to the forbidden triplet state with subsequent electron-hole annihilation (Fig. 7). This very small energy splitting results in a strong temperature dependence of the exciton lifetimes. At low temperatures (T), when $k_{\rm B}T \ll \Delta_{\rm exch}$, only the lowest triplet state is occupied and the decay time is very long, of the order of milliseconds, due to the optically forbidden character of this transition ($k_{\rm B}$: the Boltzmann constant). In the other limit, when $k_{\rm B}T \gg \Delta_{\rm exch}$, both states are equally occupied and the transition takes place mainly from the faster singlet state. Specifically, at room temperature, 75 % of the excitons are permanently in the triplet state (owing to triplet multiplicity of this state), while the exciton decay time is controlled by the indirect singlet exciton lifetime, which is several microseconds to several hundreds of microseconds long, depending on the size of the Si nanocrystals. Thus, unlike all other semiconductor nanocrystals, for Si nanocrystals, the exciton lifetime is extremely long over the entire temperature range. Since the exciton lifetime is four to five orders of magnitude longer than in other systems containing direct-bandgap semiconductor nanocrystals or quantum dots, and since the excitons persist mainly in the triplet state, Si nanocrystal assemblies seem to be favorable candidates for energy- or charge-transfer interactions.

5. Energy Transfer from Photoexcited Si **Nanocrystals to Oxygen Molecules**

5.1. Main Observations

Tischler et al. have found that the photodegradation of PSi occurs in ambient oxygen and is a result of the photo-oxidation of the PSi surface, which introduces an additional non-ra-

ADVANCED MATERIALS

diative recombination channel, Si dangling bonds.^[61] This was the first indication of the possible interaction between photoexcited Si nanocrystals and O₂. However, no distinct microscopic mechanism for PSi photodegradation and photooxidation was proposed. Later, Harper and Sailor reported the quenching of PSi emission in ambient O₂ at room temperature, and ascribed this effect to "a mechanism involving transient non-radiative electron transfer from the luminescent chromophore in porous Si to a weakly chemisorbed O₂ molecule". However, they were unable to observe the characteristic ¹O₂ emission line and attempts to chemically trap ¹O₂ also gave negative results.

Recently, we have shown that, owing to the overlap of the energy levels of Si nanocrystal assemblies and O_2 , PSi can be successfully employed for photosensitized singlet-oxygen generation. [25,63-66] We will start with a description of the interaction of excitons confined in Si nanocrystals with oxygen molecules at cryogenic temperatures. These studies allow us to monitor details of the energy-transfer process that are obscured at elevated temperatures as a result of thermal broadening effects.

Figure 8 demonstrates the strong interaction of photoexcited Si nanocrystals with oxygen molecules. To prove the universal character of this interaction we performed experiments with two ensembles of Si nanocrystals with different size distributions, and therefore different spectral positions for their PL bands. The low-temperature PL spectra of PSi measured in vacuum (Fig. 8a, dashed lines) is characterized by broad, featureless emission bands located in the visible and near-infrared spectral range of the electromagnetic spectrum. This reflects the wide bandgap distribution in the Si nanocrystal assemblies. These emission spectra are drastically modified by the physisorption of oxygen molecules (Fig. 8a, solid lines). Both emission bands are quenched and the spectra exhibit fine structure. Complete PL suppression is observed at energies above 1.63 eV (indicated by a vertical dotted line), which coincides with the ${}^{1}\Sigma$ state excitation energy. Desorption of oxygen molecules leads to a complete recovery of the initial emission properties of PSi, which indicates the reversibility of the quenching mechanism. Direct proof for the generation of ¹O₂ is the detection of light emission during its relaxation to the ${}^{3}\Sigma$ ground state of O₂. Fast relaxation of the ${}^{1}\Sigma$ state prevents the experimental observation of the ${}^{1}\Sigma - {}^{3}\Sigma$ transition.^[1] We found that quenching of the PL is always accompanied by the appearance of a narrow PL line at 0.98 eV (Fig. 8a, red PL peak) resulting from the ${}^{1}\Delta - {}^{3}\Sigma$ transition of O_2 , i.e., obviously there is energy transfer from the annihilated excitons to O_2 . This indicates that these two characteristic energies are entirely relevant to the interacting systems, the Si nanocrystal assembly and O2. We would like to mention here that the $^{1}\Delta$ - $^{3}\Sigma$ transition is the molecular electronic transition that is quite possibly the most improbable in nature because it is simultaneously spin-, orbital angular momentum, and parityforbidden.^[2] The simple fact that this transition is clearly seen spectroscopically in photoexcited micrometer-thick PSi layers is evidence for the extremely high efficiency of ¹O₂ genera-

© 2005 WILEY-VCH Verlag GmbH & Co. KGaA, Weinheim

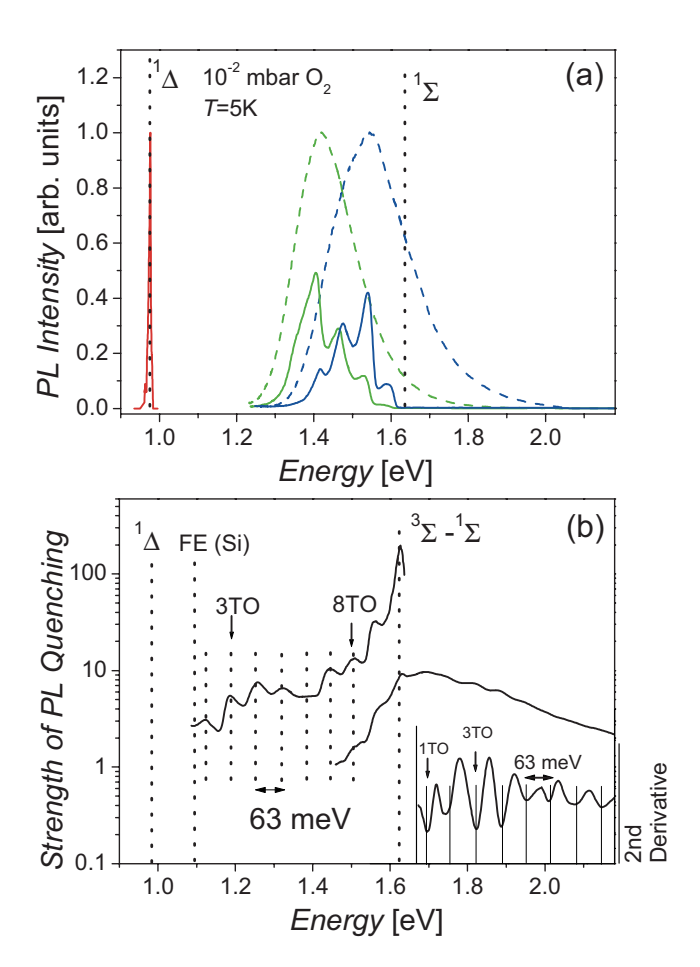


Figure 8. a) PL spectra of PSi in vacuum (dashed curves) and with oxygen molecules adsorbed at the surface (solid curves) for two samples that have different Si nanocrystal size distributions. Dashed lines indicate energies of triplet–singlet transitions of O_2 ; T=5 K, $E_{\rm ex}=2.54$ eV. b) Spectral dependence of the PL-quenching strength of PSi (T=5 K, $E_{\rm ex}=2.54$ eV). Spectroscopic features, related to multiple TO-phonon emission, are representatively labeled at two spectral positions. Energies of the free-exciton (FE) transitions of bulk Si and the $^3\Sigma^{-1}\Delta$ transition of O_2 ($^1\Delta$) are also shown by vertical dashed lines. Other vertical dashed lines are for guidance to the eye. Inset: the second derivative of the quenching strength curve above the $^3\Sigma^{-1}\Sigma$ transition of O_2 . (Reprinted with permission from [64]. Copyright 2004 The American Physical Society).

In the coupled systems, the triplet–singlet transitions of O_2 act as mid-bandgap levels that are externally introduced to the inhomogeneously broadened bandgap distribution of the nanocrystal assembly. The transfer of energy from excitons confined in Si nanocrystals to oxygen molecules is apparent from the almost complete suppression of the PL emission above 1.63 eV and the $^1\Delta$ -state emission line. Triplet–triplet annihilation during the transfer process conserves the electronic spin. However, angular momentum conservation is only fulfilled for energy transfer to the $^1\Sigma$ state, whereas the $^3\Sigma$ - $^1\Delta$ excitation requires a change of angular momentum (ΔL =2), which is forbidden in the dipole approximation. Strong coupling of excitons with the $^1\Sigma$ state leads to strong PL suppression, while only partial quenching occurs for nanocrystals that

15214095, 2005, 21, Downloaded from https://onlinelibrary.wiley.com/doi/10.1002/adma.200500328 by Egyptin Marianal Sti. Network (Enstinet), Wiley Online Library on [12.032023]. See the Terms and Conditions (https://onlinelibrary.wiejc.com/emra-and-conditions) on Wiley Online Library for rules of use; OA articles are governed by the applicable Ceravive Commons

interact weakly with the $^{1}\Delta$ state. Back transfer of energy from the $^{1}\Sigma$ state to Si nanocrystals is inhibited by its fast relaxation either to the $^{1}\Delta$ state or to the $^{3}\Sigma$ state, [67,68] whereas back energy transfer from the ${}^{1}\Delta$ state is impossible since its energy is below the bandgap of bulk Si. We note that for physisorbed oxygen molecules, the energies of the infrared $^{1}\Delta$ emission line (0.973 eV, Fig. 8a) and of the PL onset (1.619 eV, Fig. 8a) are lower than those known for gaseous oxygen, being 0.98 and 1.63 eV, respectively. The weak van der Waals' interaction of adsorbed oxygen molecules with Si surface atoms lowers the energy of the excited states of O₂ and slightly broadens the transitions. Thus, optical spectroscopy allows for an accurate measurement of the O₂ physisorption energy.

As follows from Figure 8a, the exact shape of the quenched PL spectra is defined by a convolution of the "envelope function", i.e., the Si nanocrystal size distribution, and the spectral dependence of the coupling efficiency between excitons and O₂. To eliminate the influence of the size distribution on the shape of the quenched PL spectrum, we define the strength of quenching as the ratio of the PL intensity measured in vacuum to that measured under quenched conditions. To monitor exciton coupling to the $^{1}\Sigma$ state of O_{2} a relatively weak PL quenching level was achieved. Figure 8b demonstrates the results of this procedure. To resolve the weak spectral modulation of the curve covering the energy region above the $^{1}\Sigma$ state, its second derivative was used.

The spectral dependence of the PL suppression strength allows for a detailed description of the energy-transfer mechanism. The strongest PL quenching level and the most efficient energy transfer is found for nanocrystals that have bandgap energies that coincide with the ${}^{3}\Sigma^{-1}\Sigma$ transition of O₂. Since Si nanocrystals have an indirect band structure, under ordinary conditions they luminesce 56 meV below their bandgap owing to the emission of momentum-conserving TO phonons (Fig. 5). Therefore, when energy is efficiently transferred from the exciton, an additional maximum in the quenching strength is observed 56 meV below the energy of the ${}^{3}\Sigma^{-1}\Sigma$ transition. It is evident from Figure 8b that nanocrystals whose bandgaps do not resonantly match the excitation energies of the O2 singlet states participate in the energy transfer as well. The excess exciton energy with respect to the energies of the ${}^{1}\Delta$ and ${}^{1}\Sigma$ states is released by the emission of phonons. In Figure 9 the mechanism of energy transfer from excitons to O2 is sketched. Since real electronic states below the nanocrystal bandgap are absent, energy dissipation should be governed by multiphonon emission. This process is most probable for phonons that have the highest density of states, which in bulk Si are TO phonons, which are almost at the centrum of the Brillouin zone with an energy of 63 meV. [69] If the bandgap energy of Si nanocrystals does not coincide with the excitation energy of an O₂ singlet state plus an integer multiple of the energy of those phonons, an additional emission of acoustic phonons is required for the conservation of energy. This process has a smaller probability and the efficiency of energy exchange is reduced. Consequently, equidistant maxima and minima appear in the spectral dependence of the quenching strength, which provide experimental evidence for phonon-assisted energy transfer (for clarity see Fig. 9, where the details of the energy-transfer process are summarized). These energy-transfer resonances can be spectrally resolved due to a singularity in the phonon density of states.

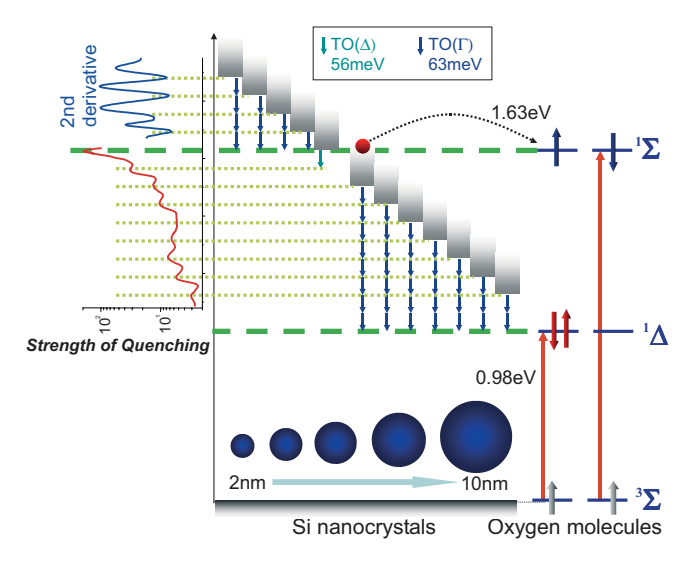


Figure 9. Sketch of the energy-level diagram of O2, and different groups of Si nanocrystals participating in the electron-exchange process most efficiently. The principal steps occurring in the energy-transfer process are shown. Energy exchange occurs when a photoexcited electron (indicated by the red sphere), initially belonging to a nanocrystal, is exchanged with a non-excited electron initially belonging to O2 (indicated by the gray arrow). This process results in the formation of singlet O2 states and compensation of the holes confined in Si nanocrystals. Participation of a number of energy-conserving TO phonons is indicated by blue vertical arrows. The momentum-conserving TO phonon is marked by a light-blue

5.2. Mechanism of Energy Transfer

Basically, dipole-dipole (Förster transfer)^[9] or direct-electron-exchange (Dexter transfer)[10] coupling can account for energy transfer from excitons confined in Si nanocrystals to O2. Since long-range multipole interaction is based on optically allowed transitions of the donor and acceptor, it is unlikely to be applied to the triplet-triplet annihilation of excitons and O₂ followed by singlet-oxygen creation. However, in the electron-exchange mechanism these spin restrictions are lifted, and triplet-exciton annihilation accompanied by the spin-flip excitation of an oxygen molecule is an allowed process. [69] The energy-transfer rate is defined by the spatial overlap of the electronic wavefunctions of the interacting species and depends exponentially on the donor-acceptor distance. [10] The advantage of our system is that a controlled variation of the donor-acceptor separation is possible by modification of the nanocrystal surfaces.

The surfaces of nanocrystals play a key role in virtually all of their properties, from light emission to solubility of nanocrys-

tals in water. Specifically for Si nanocrystals, three completely different types of surfaces can be realized. As-prepared PSi has a H-terminated surface (see vibrational modes of the Si-H bond, inset to Fig. 10a, solid line). Thermal annealing of PSi in air at temperatures below 300 °C results in the incorporation of a monolayer of oxygen atoms back-bonded to the surface of the nanocrystals while hydrogen atoms still remain

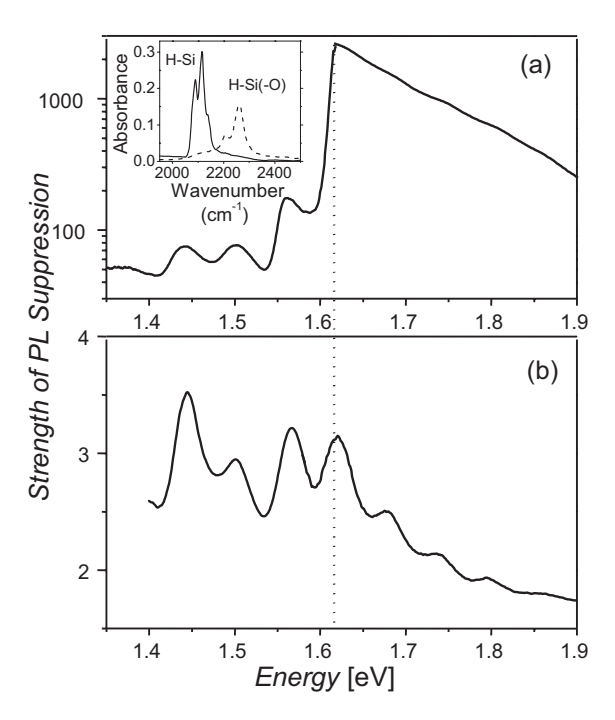


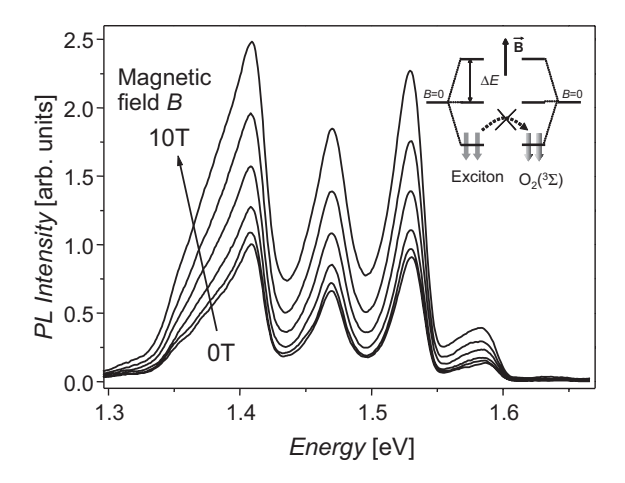
Figure 10. Spectral dependence of the PL-quenching strength for a) as-prepared and b) oxidized PSi at equal oxygen ambient pressures (10^{-2} mbar; 1.0 Pa). T=5 K, $E_{\rm ex}=2.54$ eV. Inset: infrared absorption spectra showing the Si-H bond in PSi. Solid line: as-prepared, H-terminated PSi. Dotted line: thermally oxidized PSi containing back-bonded oxygen at the surface of Si nanocrystals. (Reprinted with permission from [63] and [64]. Copyright 2003 and 2004 The American Physical Society).

at the surface (hydrogen passivation of the surface is still preserved;^[70] inset to Fig. 10a, dotted line). At annealing temperatures above 700 °C, the surface of the nanocrystal can be completely oxidized. For Si nanocrystals that have a monolayer of back-bonded oxygen, the increased spacing between confined excitons and adsorbed oxygen molecules is on the order of 3 Å (double the length of the Si-O bond).^[71] A monolayer of incorporated oxygen also implies an additional potential barrier for the mutual tunnelling of electrons. This critically affects the efficiency of the electron-exchange interaction. Contrary to strong coupling for H-terminated nanocrystals (Fig. 10a), the PL-quenching efficiency (and electron-exchange rate) is reduced by orders of magnitude if a thin oxide barrier is present (Fig. 10b). We would like to note that because the transition from H-terminated to O-terminated surfaces can be achieved smoothly via successive nanocrystal surface oxidation, the photosensitizing efficiency of Si nanocrystal assemblies, unlike other systems, can be accurately controlled.

© 2005 WILEY-VCH Verlag GmbH & Co. KGaA, Weinheim

5.3. Control of the Energy-Exchange Efficiency via Electron-Spin Manipulation

For the direct electron-exchange process, mutual alignment of the electron spins is crucial. Therefore, we have performed additional experiments allowing for the manipulation of the electron spins of excitons and O2. While the involved transitions are spin-forbidden in isolated Si nanocrystals and oxygen molecules, they become allowed through the exchange interaction. For the energy transfer to occur, the exchanged electrons must have opposite mutual spin orientation. To demonstrate the influence of spin statistics on the energytransfer rate, we measured the magnetic-field dependence of the PL-quenching efficiency (Fig. 11). If no magnetic field is present, the energy levels of the triplet excitons and the triplet ground state of O2 are threefold degenerate and populated with equal probability. Thus, the spin requirements are fulfilled for all the excitons and all the oxygen molecules, and



15214095, 2005, 21, Downloaded from https://onlinelibrary.iley.com/doi/1.01002adma_200500328 by Egyptin Marianal St. Network (Estinated, Wiley Online Library on 1120302033). See the Terms and Conditions (https://onlinelibrary.wiely.com/terms-and-conditions) on Wiley Online Library for rules of use; OA articles are governed by the applicable Creative Commons

Figure 11. Quenched PL spectrum of PSi at various magnetic fields. T=4.2 K, E_{ex} =2.54 eV. Inset: Zeeman splitting of the triplet exciton state and the ${}^{3}\Sigma$ triplet ground state of molecular oxygen. The spin orientations for electrons in the lowest lying levels are indicated by arrows. Energy transfer from exciton to the ground state of O2 via electron exchange between these states is prohibited due to their parallel spin alignment. (Reprinted with permission from [64]. Copyright 2003 The American Physical Society).

energy transfer occurs most efficiently. A magnetic field introduces a common quantization axis for the spins and the degeneracy is lifted (inset to Fig. 11). Raising the magnetic field increases the Zeeman splitting $(\Delta E_Z)^{[60,72]}$

$$\Delta E_{\rm Z} = g\mu_{\rm B} H \left(g_{\rm exciton} \sim g_{\rm oxygen} \sim 2 \right) \tag{1}$$

and the occupation number of the thermally populated higher lying states decreases. Here, g is the g-factor, $\mu_{\rm B}$ is the Bohr magneton, and H is the magnetic field. At low temperatures, a magnetic field results in the preferential occupation of "spin-down" states for both O₂ and excitons, while, to realize

energy exchange, "spin-up states" are required (see sketch in Fig. 11). For magnetic fields of 10 T and temperatures below 10 K, the relevant energies

$$k_{\rm B}T \sim \Delta E_{\rm Z} \sim 1 \text{ meV}$$
 (2)

are comparable and a significant reduction of the PL quenching, i.e., energy-exchange efficiency, is observed. In the limit of T=0 K, energy exchange between excitons and O_2 would be completely prohibited in the presence of an external magnetic field. Thus, remarkably, a very small magnetic energy (~1 meV) can efficiently control energy-exchange processes on a scale of electronvolts by aligning the spins of the interacting species.

5.4. Energy Transfer at Elevated Temperatures

Spectroscopic experiments at cryogenic temperatures allow clarification of the details of the energy-transfer mechanism. However, this is mostly of academic interest. Of more practical interest is the generation of singlet O2 at elevated temperatures, owing to the role played by singlet O₂ in photochemical reactions and biology/medicine. [1,2,4,6,7] Figure 12 shows the strength of PL quenching obtained by dividing the intensities of PL spectra taken in vacuum by those in ambient oxygen gas at 150 and 295 K. Unlike at cryogenic temperatures, conditions for optimal exciton-O2 interaction are not fulfilled. A small spatial separation is realized only dur-

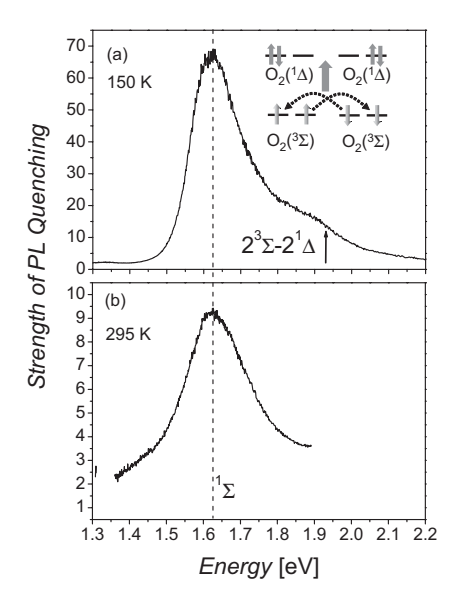


Figure 12. Spectral dependence of the quenching strength of PSi emission in ambient oxygen gas. a) T=150 K, b) T=295 K, O_2 pressure is 1 bar, $E_{\rm ex}$ = 2.54 eV. The energy positions of the O_2 dimer transitions $(2^3\Sigma-2^1\Delta)$ and the $^3\Sigma-^1\Sigma$ transition are indicated. Inset: schematic illustration of spin-conserving electron exchange between two $^{3}\Sigma$ states.

ing the short time of collisions between oxygen molecules and the nanocrystal surface. Additionally, the exciton lifetime and the occupation number of the spin-triplet state of the exciton decreases with increasing temperature. [23] Therefore, a weaker PL suppression that scales with the collision rate, i.e., the gas pressure, is obtained, and energy transfer to the ${}^{1}\Sigma$ state is seen as a relatively broad spectral resonance. At an intermediate temperature, T = 150 K, a second spectral feature in the spectral region of ~1.75-1.95 eV is observed, which becomes more pronounced with increasing oxygen concentration (Fig. 12a). We attribute this to energy transfer from excitons confined in Si nanocrystals to O2 dimers (simultaneous excitation of two neighboring oxygen molecules). The O2 dimer is known to be a complex of groundstate oxygen molecules induced by weak van der Waals' interaction.^[73] The discrete electronic transition for O₂ dimers, corresponding to $2 \times (^{1}\Sigma^{-1}\Delta)$ energy, should occur at ~1.95 eV (indicated by arrow), and is thermally and collisionally broadened in the gas phase.^[71] Excitation of the O₂ dimer involves spin-conserving electron exchange among the two $^{3}\Sigma$ states, whereas the exciton provides the energy to activate the process. Consequently, the PL of PSi is quenched in the considered spectral range, and according to our observations, energy transfer to the dimer state is enhanced at higher pressures due to an increased probability for O₂ dimer formation. As a result of thermal dissociation of the complex (dissociation energy of the O₂ dimer is ~10 meV),^[74] a continuous decrease of the dimer-related quenching band is observed when the temperature is increased. For temperatures higher than 250 K, energy transfer to the O₂ dimer cannot be resolved spectroscopically. We would like to note that the efficiency of singlet-O2 generation is usually defined as the ratio of the number of incident photons to the number of generated singlet-oxygen molecules. Direct excitation of O2 dimers implies that one photon, in general, can create two singlet-oxygen molecules. Therefore, theoretically, ¹O₂ generation efficiency in our system can exceed 100%.

The most important parameter for any system capable of producing singlet oxygen is its efficiency at room temperature. As we have already mentioned, each exciton that is lost from the light emission process necessarily produces a singlet-oxygen molecule. The PL suppression level measured in the presence of ambient O₂ at 1 bar is shown in Figure 12b. Thermalbroadening effects do not allow for clear observation of the fine details of the energy-transfer process, but again, excitons that have energies in the vicinity of the ${}^{3}\Sigma^{-1}\Sigma$ transition most efficiently excite O₂. The suppression of the PL intensity at room temperature is equal to 9, which implies that nearly 90% of the photoexcited excitons transfer their energy to oxygen molecules. This allows us to estimate the generation rate of singlet O₂ at room temperature in the pores of PSi. At ambient O₂ pressure and 1 W cm⁻² excitation intensity, the generation rate is calculated to be $\sim 5 \times 10^{20}$ (singlet-oxygen molecules) cm⁻³ s⁻¹.

5.5. Singlet-Oxygen Generation in Liquids

For many practical applications of singlet oxygen, its generation in liquids at room temperature is required. One of the standard methods to detect singlet oxygen in liquid is to use a biochemical trap (singlet-oxygen acceptor) and to analyze a specific reaction product or monitor the decrease in the acceptor material. Typical biochemical traps are cholesterol, 1,3-diphenylisobenzofuran, p-nitrosodimethylalanine, sodium azide, etc. [7,8,66,75,76] However, these provide only indirect evidence. Direct evidence of singlet-oxygen generation in solutions can only be obtained via detection of the PL line that results from the $^{1}\Delta$ to $^{3}\Sigma$ transition. Fortunately, in solution, intermolecular interactions lead to strong enhancement of the transition probability. The radiative transition rate is three to four orders of magnitude larger in solution than in a dilute gas phase. [77] However, in most solvents, deactivation of ¹O₂ is radiationless due to collisional electronic-vibrational energy transfer from ¹O₂ to an oscillator of a solvent molecule; i.e., the electronic excitation energy of ¹O₂ is converted into vibrational energy of the ground state of O2 and a solvent molecule. The most probable energy-accepting oscillators in solvent molecules are their terminal atom pairs with the highest vibrational energy (for instance O-H, C-H). [78,79] Molecules composed of low-energy oscillators such as C-F and C-Cl act as poor quenchers whereas those with high-energy oscillators such as O-H and C-H are strong quenchers. In fact, the lifetime of singlet oxygen in the lowest excited state, ${}^{1}O_{2}$ (${}^{1}\Delta$), varies over a wide range, from 4 µs to 100 ms, depending on the type of solution.^[78,79] Therefore, to obtain reliable PL data, solvents consisting of poor quenchers must be chosen. The other important selection criterion for the solvent is that it should not quench the luminescence of Si nanocrystals. Hexafluorobenzene (C₆F₆) is a molecule that fulfils all these conditions. The singlet-oxygen lifetime in C₆F₆ is about 21 ms, [2] which is about three orders of magnitude longer than that in benzene and four orders of magnitude longer than that in water. [2] A schematic illustration of the experimental setup employed to detect singlet-oxygen generation in solution is sketched in the inset to Figure 13. Powdered PSi that was prepared via the mechanical decomposition of PSi layers in an ultrasound bath was placed into a quartz cell filled with C₆F₆. The cell was irradiated from the front surface and the PL was collected from the same surface.

Figure 13 shows the PL spectrum of PSi powder dispersed in C₆F₆ solution at room temperature. The broad emission band centered at around 1.65 eV arises from the recombination of excitons in Si nanocrystals. In addition to the band, a weak peak can be observed at around 0.975 eV. This peak disappears when the solution is bubbled with N2 gas, and becomes larger on bubbling with O2 gas. This emission line can thus be assigned to the radiative relaxation of ${}^{1}O_{2}$ (${}^{1}\Delta$) dissolved in C₆F₆. It is worth noting that the 0.975 eV PL is much weaker when benzene is used as the solvent instead of C₆F₆. Strong emission from ${}^{1}O_{2}$ (${}^{1}\Delta$) is observed only when the H-terminated PSi powder is dispersed. The $^{1}\Delta$ PL intensity for

© 2005 WILEY-VCH Verlag GmbH & Co. KGaA, Weinheim

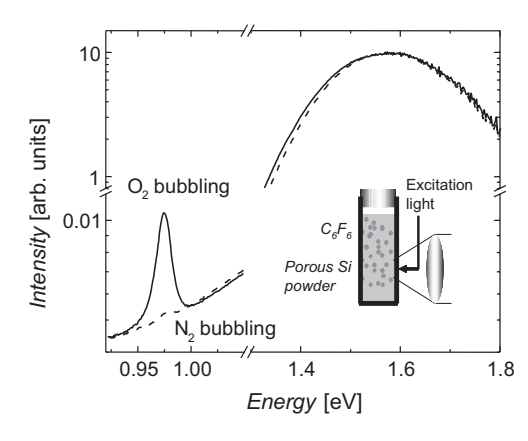


Figure 13. PL spectra of PSi powder dispersed in O₂-saturated (bubbling at 1 bar of O2 ambient, solid line) and O2-free (dashed line) C6F6 solution at room temperature. E_{ex} = 2.54 eV. The peak at around 0.975 eV corresponds to emission from singlet oxygen. The experimental setup is shown in the inset. (Reprinted with permission from [66]. Copyright 2004 The American Physical Society).

1521495, 2005, 21, Downloaded from https://onlinelibrary.wiley.com/doi/10.1002/adma.20000328 by Egytian National Sti. Network (Enstinet), Wiley Online Library on [12.03/2023]. See the Terms and Conditions (https://onlinelibrary.wiley.com/emms

and-conditions) on Wiley Online Library for rules of use; OA articles are governed by the applicable Creative Commons

a solution containing oxidized powder is much smaller than for a solution containing fresh powder. [65]

Direct evidence for the photosensitized formation of singlet oxygen is obtained from PL excitation spectra. In Figure 14, the intensity of the singlet-oxygen PL is plotted as a function of the excitation energy. We can see that singlet oxygen can be generated by light over a broad range of wavelengths

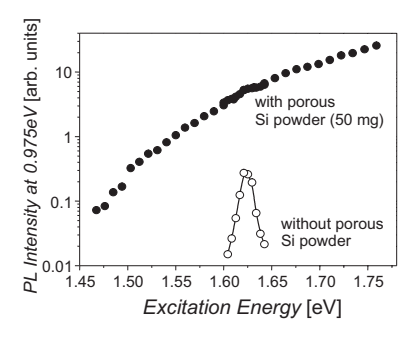


Figure 14. PL intensity of the singlet oxygen $^{1}\Delta - ^{3}\Sigma$ line as a function of excitation energy for O₂-saturated C₆F₆ containing PSi powder (filled circles) and for O_2 -saturated C_6F_6 without powder (open circles). T = 295 K. (Reprinted with permission from [66]. Copyright 2004 The American Physical Society).

(700–850 nm, in this spectral range photons can penetrate relatively deep into human tissue). This broad excitation spectrum is apparently different from that obtained for pure C₆F₆ in which singlet oxygen can be generated by excitation light, which is exactly energetically resonant with the $^{3}\Sigma$ to $^{1}\Sigma$ transition. The broad excitation spectrum thus provides direct evidence for the indirect excitation of singlet oxygen by energy transfer from Si nanocrystals.

The very broad excitation spectrum covering a part of the near-infrared and the entire visible range of the electromag-

netic spectrum provides a significant advantage for systems containing Si nanocrystals in some applications. For example, as mentioned in Section 1, the absorption maxima of dye photosensitizers used for the photodynamic therapy of cancer are between 630 and 700 nm. Photons in this spectral range penetrate only a few millimeters into tissue. On the other hand, Si nanocrystals can mediate generation of ¹O₂ under illumination by light having a longer wavelength. It may significantly extend the applicability of photodynamic therapy if Si nanocrystals could be used as photosensitizers of O_2 .

In Figure 14, in the PL excitation spectrum of a solution containing PSi powder, a small bump can be seen at around 1.63 eV. This bump corresponds to the direct excitation of oxygen molecules. The bump becomes more pronounced at higher excitation power, suggesting that the excitation power dependence is completely different for direct and indirect ¹O₂ excitation processes. In fact, with PSi powder, the ¹O₂ PL intensity is saturated at very low excitation power. The absorption cross-section of O2 is extremely small even for light of the exact resonant energy. On the other hand, the strong saturation of ¹O₂ PL intensity for the solution containing PSi powder suggests that the energy-transfer rate is so large that almost all the O_2 available in solution is converted to 1O_2 . The lifetime of generated singlet oxygen can be estimated from a decay curve of the singlet-oxygen PL. The lifetime is found to be about 3.9 ms, [65] which is shorter than the literature value (21 ms).^[2] The shortening of the lifetime may result from the collisions of singlet oxygen with the walls of porous Si pores and the resultant non-radiative relaxation, because a majority of the singlet oxygen is generated in the pores. Therefore, for the practical application of Si nanocrystals as singlet-oxygen generators, smaller grain sizes of PSi powder or Si nanocrystal colloids are desirable.

For the application of singlet oxygen in the photodynamic therapy of cancer, disinfection of bacteria, etc., its generation in aqueous solution is crucial. Unfortunately, the very short lifetime of ¹O₂ in water (3.1 μs), due to fast non-radiative relaxation processes, makes the detection of PL from ¹O₂ dissolved in water very difficult. However, even if the PL is not detected, energy transfer can be indirectly probed by monitoring the lifetime of the exciton PL. In Figure 15, PL decay curves detected at 1.63 eV for porous Si powder immersed in water are shown. In O₂-free solutions, the lifetime is 90 μs, while in O₂-saturated solutions, it is significantly shorter (40 μs). This shortening of the lifetime is a result of energy transfer to oxygen molecules dissolved in water, which is evidence for the formation of singlet oxygen. Spectral dependence of the PL suppression level demonstrates a broad band centered at 1.63 eV, similar to that measured in ambient gaseous O_2 (Fig. 12b).

6. Conclusions

The enormous range of entirely new physical properties afforded by size tuning of semiconductor nanocrystals has drawn the attention of scientists from different disciplines,

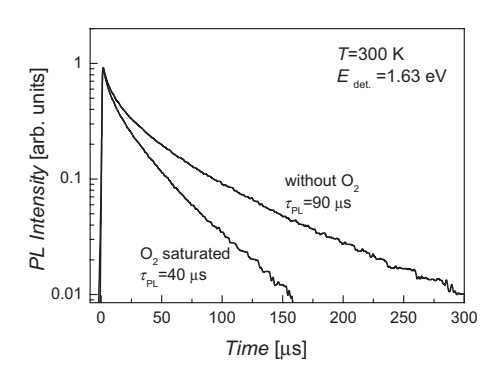


Figure 15. PL decay curves of porous Si immersed in O2-saturated (bubbling at 1 bar of O2 ambient) and O2-free water detected at 1.63 eV $(E_{\text{det.}})$. T = 295 K, $E_{\text{ex}} = 3.67$ eV.

from physical chemists to materials scientists and from condensed-matter physicists to electrical engineers. The potential applications of these materials are now well established in the above-mentioned disciplines. Additional emerging fields for the application of semiconductor nanocrystals include biology and medicine. In particular, a large amount of effort has been directed toward making nanosilicon a biologically relevant material. [80] Si nanocrystals can be considered as chemical reagents, which may be dissolved in a fluid containing organic molecules or biological objects. The generation rate of singlet oxygen scales with the quantum yield of the photosensitizer PL. Nanocrystal assemblies are believed to have the potential to be ideal chromophores. Specifically for Si nanocrystals, the luminescence quantum yield can be high if the surface chemistry is controlled. Controllable chemical functionalization of Si-nanocrystal surfaces suggests that the unique electronic properties of Si nanocrystals can be tailored in a determinable manner. [80] However, despite surface-termination effects that are well understood, Si nanocrystals are still not ideal chromophores. On the other hand, Si-nanocrystal sensitizers can be produced in large amounts chemically in a completely controllable manner from fine Si powder. This can be achieved without lithographic or epitaxial techniques, which are the conventional methods for realizing semiconductor nanostructures. From the point of view of practical applications, especially in medicine, Si nanocrystals in colloidal form should act in a similar way to conventional dye molecules. Finally, we believe that this research represents a step towards functionalization of the most commercially used semiconductor for chemical, biological, and medical applications.

> Received: February 14, 2005 Final version: June 22, 2005 Published online: September 29, 2005

^[1] N. J. Turro, Modern Molecular Photochemistry, University Science Books, Sausalito, CA 1991.

C. Schweitzer, R. Schmidt, Chem. Rev. 2003, 103, 1685.

H. Kautsky, H. DeBruijn, Naturwissenschaften 1931, 19, 1043. [3]

D. L. Gilbert, C. A. Colton, Reactive Oxygen Species in Biological System, Plenum, New York 1999.

ADVANCED MATERIALS

- [5] M. C. DeRosa, R. J. Crutchley, Coord. Chem. Rev. 2002, 233–234, 351.
- [6] J. G. Moser, *Photodynamic Tumor Therapy: 2nd and 3rd Generation Photosensitizers*, Gordon and Breach, London **1998**.
- [7] Methods in Enzymology, Singlet Oxygen, UV-A, and Ozone (Eds: L. Packer, H. Sies), Academic, London 2000, p. 319.
- [8] D. B. Min, J. M. Boff, Compr. Rev. Food Sci. Food Saf. 2002, 1, 58.
- [9] T. Förster, Ann. Phys. (N. Y.) 1948, 2, 55.
- [10] D. L. Dexter, J. Chem. Phys. 1953, 21, 836.
- [11] S. Wang, R. Gao, F. Zhou, M. Selke, J. Mater. Chem. 2004, 14, 487.
- [12] M. K. Nissen, S. M. Wilson, M. L. W. Thewalt, Phys. Rev. Lett. 1992, 69, 2423.
- [13] J. W. Arbogast, A. P. Darmanyan, C. S. Foote, Y. Rubin, F. Diederich, M. M. Alvarez, S. J. Anz, R. L. Whetten, J. Phys. Chem. 1991, 95 11
- [14] a) N. Tagmatarchis, H. Kato, H. Shinohara, *Phys. Chem. Chem. Phys.* **2001**, *3*, 3200. b) N. Tagmatarchis, H. Shinohara, *Org. Lett.* **2000**, 2, 3551.
- [15] P. Cheng, S. R. Wilson, D. I. Schuster, Chem. Commun. 1999, 89.
- [16] a) A. I. Ekimov, A. A. Onushchenko, Fiz. Tekh. Poluprovodn. 1982, 16, 1215. b) A. I. Ekimov, A. A. Onushchenko, Sov. Phys.—Semicond. 1982, 16, 775.
- [17] R. Rossetti, S. Nakahara, L. E. Brus, J. Chem. Phys. 1983, 79, 1086.
- [18] Special Issue on Spectroscopy of Isolated and Assembled Semiconductor Nanocrystals, J. Lumin. 1996, 70, 1.
- [19] A. P. Alivisatos, J. Phys. Chem. 1996, 100, 13226.
- [20] M. Nirmal, D. J. Norris, M. Kuno, M. G. Bawendi, Phys. Rev. Lett. 1995, 75, 3728.
- [21] M. Nirmal, L. Brus, Acc. Chem. Res. 1999, 32, 407.
- [22] A. C. S. Samia, X. Chen, C. Burda, J. Am. Chem. Soc. 2003, 125, 15737
- [23] A. G. Cullis, L. T. Canham, P. D. J. Calcott, J. Appl. Phys. 1997, 82, 909.
- [24] D. Kovalev, H. Heckler, G. Polisski, F. Koch, Phys. Status Solidi B 1999, 215, 871.
- [25] D. Kovalev, E. Gross, N. Künzner, F. Koch, V. Y. Timoshenko, M. Fujii, *Phys. Rev. Lett.* **2002**, 89, 137 401.
- [26] L. Brus, in Semiconductors and Semimetals (Ed: D. J. Lockwood), Academic, New York 1996.
- [27] M. Fujii, M. Yoshida, Y. Kanzawa, S. Hayashi, K. Yamamoto, *Appl. Phys. Lett.* **1997**, 71, 1198.
- [28] P. G. Kik, A. Polman, J. Appl. Phys. 2000, 88, 1992.
- [29] M. Zacharias, L. X. Yi, J. Heitmann, R. Scholz, M. Reiche, U. Gösele, Solid State Phenom. 2003, 94, 95.
- [30] G. F. Grom, D. J. Lockwood, J. P. Mccaffrey, H. J. Labbe, P. M. Fauchet, B. White, J. Diener, D. Kovalev, F. Koch, L. Tsybeskov, *Nature (London)* 2000, 407, 358.
- [31] F. Huisken, G. Ledoux, O. Guillois, C. Reynaud, Adv. Mater. 2002, 14, 1861.
- [32] L. T. Canham, Appl. Phys. Lett. 1990, 57, 1046.
- [33] V. Lehmann, U. Gösele, Appl. Phys. Lett. 1991, 58, 856.
- [34] O. Bisi, S. Ossicini, L. Pavesi, Surf. Sci. Rep. 2000, 38, 1.
- [35] V. Lehmann, R. Stengl, A. Luigart, *Mater. Sci. Eng. B* 2000, 69–70, 11.
- [36] A. J. Steckl, J. Xu, H. C. Mogul, Appl. Phys. Lett. 1992, 62, 2111.
- [37] G. Anaple, R. Burrows, Y. Wu, P. Boolchand, J. Appl. Phys. 1995, 78, 4273.
- [38] A. G. Cullis, L. T. Canham, Nature (London) 1991, 353, 335.
- [39] R. Herino, in *Properties of Porous Silicon* (Ed: L. Canham), INSPEC, London 1997, p. 89.
- [40] P. D. J. Calcott, K. J. Nash, L. T. Canham, M. J. Kane, D. Brumhead, J. Phys.: Condens. Matter 1993, 5, L91.

- [41] T. Suemoto, K. Tanaka, A. Nakajima, T. Itakura, Phys. Rev. Lett. 1993, 70, 3659.
- [42] A. Kux, M. Ben-Chorin, Thin Solid Films 1996, 276, 272.
- [43] M. Rosenbauer, M. Stutzmann, S. Finkbeiner, J. Weber, E. Bustarret, *Phys. Rev. B* 1997, 55, 10117.
- [44] D. Kovalev, H. Heckler, M. Ben-Chorin, G. Polisski, M. Schwartzkopff, F. Koch, *Phys. Rev. Lett.* 1998, 81, 2803.
- [45] Y. Kanemitsu, S. Okamoto, Phys. Rev. B 1998, 58, 9652.
- [46] M. S. Hybertsen, Phys. Rev. Lett. 1994, 72, 1514.
- [47] S. Gardelis, J. S. Rimmer, P. Dawson, B. Hamilton, R. A. Kubiak, T. E. Whall, E. H. C. Parker, Appl. Phys. Lett. 1991, 59, 2118.
- [48] J.-C. Vial, A. Bsiesy, F. Gaspard, R. Herino, M. Ligeon, F. Muller, R. Romestain, R. M. Macfarlane, *Phys. Rev. B* 1992, 45, 14171.
- [49] J. Diener, D. Kovalev, G. Polisski, H. Heckler, F. Koch, *Phys. Status Solidi B* 1999, 214, R13.

1521 4095, 2005, 21, Downloaded from https://onlinelibrary.wiley.com/doi/10.1002/adma.200500328 by Egyptian National Sti. Network (Enstinet), Wiley Online Library on [12.032023]. See the Terms

and Conditions (https://onlinelibrary.

ons) on Wiley Online Library for rules of use; OA articles are governed by the applicable Creative Comm

- [50] J. C. Merle, M. Capizzi, P. Fiorini, A. Frova, Phys. Rev. B 1978, 17, 4821.
- [51] M. Nirmal, D. J. Norris, M. Kuno, M. G. Bawendi, Al. Efros, M. Rosen, *Phys. Rev. Lett.* **1995**, 75, 3728.
- [52] D. Gammon, E. S. Snow, B. V. Shanabrook, D. S. Katzer, D. Park, Phys. Rev. Lett. 1996, 76, 3005.
- [53] M. Bayer, O. Stern, A. Kuther, A. Forchel, Phys. Rev. B 2000, 61, 7273.
- [54] T. Takagahara, Phys. Rev. B 1993, 47, 4569.
- [55] T. Takagahara, Phys. Rev. B 1996, 53, R4205.
- [56] E. Martin, C. Delerue, G. Allan, M. Lannoo, Phys. Rev. B 1994, 50, 18258.
- [57] A. Franceschetti, A. Zunger, Phys. Rev. Lett. 1997, 78, 915.
- [58] G. Fishman, R. Romestain, J.-C. Vial, J. Phys. IV 1993, C5, 355.
- [59] K. J. Nash, P. D. J. Calcott, L. T. Canham, R. J. Needs, *Phys. Rev. B* 1995, 51, 17 698.
- [60] H. Heckler, D. Kovalev, G. Polisski, N. N. Zinov'ev, F. Koch, Phys. Rev. B 1999, 60, 7718.
- [61] M. A. Tischler, R. T. Collins, J. H. Stathis, J. C. Tsang, Appl. Phys. Lett. 1992, 60, 639.
- [62] J. Harper, M. J. Sailor, Langmuir 1997, 13, 4652.
- [63] E. Gross, D. Kovalev, N. Künzner, J. Diener, F. Koch, V. Y. Ti-moshenko, M. Fujii, *Phys. Rev. B* 2003, 68, 115 405.
- [64] D. Kovalev, E. Gross, V. Y. Timoshenko, M. Fujii, Appl. Phys. Lett. 2004, 85, 3590.
- [65] M. Fujii, S. Minobe, M. Usui, S. Hayashi, E. Gross, J. Diener, D. Ko-valev, *Phys. Rev. B* 2004, 70, 085 311.
- [66] M. Fujii, M. Usui, S. Hayashi, E. Gross, D. Kovalev, N. Künzner, J. Diener, V. Y. Timoshenko, J. Appl. Phys. 2004, 95, 3689.
- [67] R. Schmidt, M. Bodesheim, J. Phys. Chem. A 1998, 102, 4769.
- [68] A. Damjanovic, T. Ritz, K. Schulten, Phys. Rev. E 1999, 59, 3293.
- [69] W. Weber, Phys. Rev. B 1977, 15, 4789.
- [70] P. Gupta, V. L. Colvin, S. M. George, Phys. Rev. B 1988, 37, 8234.
- [71] CRC Handbook of Chemistry and Physics, 78th ed. (Ed: D. R. Linde), CRC Press, New York 1997–1998.
- [72] D. R. Kearns, A. J. Stone, J. Chem. Phys. 1971, 55, 3383.
- [73] A. U. Khan, M. Kasha, J. Am. Chem. Soc. 1970, 92, 3293.
- [74] J. O. Hirschfelder, C. F. Curtiss, R. B. Bird, Molecular Theory of Gases and Liquids, Wiley, New York 1954.
- [75] R. H. Young, K. Wehrly, R. L. Martin, J. Am. Chem. Soc. 1971, 93, 5774.
- [76] M. Nowakowska, M. Kepczyński, K. Szczubiatka, Macromol. Chem. Phys. 1995, 196, 2073.
- [77] M. Hild, R. Schmidt, J. Phys. Chem. A 1999, 103, 6091.
- [78] R. Schmidt, J. Am. Chem. Soc. 1989, 111, 6983.
- [79] R. Schmidt, F. Shafii, M. Hild, J. Phys. Chem. 1999, 103, 2599.
- [80] J. M. Buriak, Chem. Rev. 2002, 102, 1271.